

AD-A275 365**DOCUMENTATION PAGE**Form Approved
OMB No. 0704-0188

This report contains information that may be exempt from public release under the Freedom of Information Act (5 U.S.C. 552). It is the policy of the Department of Defense to make available to the public information that is not exempt from public release. This report is being made available to the public in accordance with the provisions of the Freedom of Information Act. It is the policy of the Department of Defense to make available to the public information that is not exempt from public release. This report is being made available to the public in accordance with the provisions of the Freedom of Information Act.

2. REPORT DATE

FEB 1993

3. REPORT TYPE AND DATES COVERED

THESIS/DISSERTATION

4. TITLE AND SUBTITLE

SYNTHETIC IMAGE GENERATOR MODEL: APPLICATION OF VIEW
ANGLE DEPENDENT REFLECTIVITY COMPONENTS AND PERFORMANCE
EVALUATION IN THE VISIBLE REGION

5. FUNDING NUMBERS

6. AUTHOR(S)

RICHARD B. STARK

7. PERFORMING ORGANIZATION NAME(S) AND ADDRESS(ES)

AFIT Student Attending: ROCHESTER INSTITUTE OF TECHNOLOGY

8. PERFORMING ORGANIZATION
REPORT NUMBER

AFIT/CI/CIA- 93-158

9. SPONSORING/MONITORING AGENCY NAME(S) AND ADDRESS(ES)

DEPARTMENT OF THE AIR FORCE
AFIT/CI
2950 P STREET
WRIGHT-PATTERSON AFB OH 45433-7765

10. SPONSORING/MONITORING
AGENCY REPORT NUMBER

11. SUPPLEMENTARY NOTES

DTIC
ELECTE
FEB 04 1994

12a. DISTRIBUTION/AVAILABILITY STATEMENT

Approved for Public Release IAW 190-1
Distribution Unlimited
MICHAEL M. BRICKER, SMSgt, USAF
Chief Administration

12b. DISTRIBUTION CODE

13. ABSTRACT (Maximum 200 words)

8896 94-03969



94 2 03 183

14. SUBJECT TERMS

15. NUMBER OF PAGES

62

16. PRICE CODE

17. SECURITY CLASSIFICATION
OF REPORT18. SECURITY CLASSIFICATION
OF THIS PAGE19. SECURITY CLASSIFICATION
OF ABSTRACT

20. LIMITATION OF ABSTRACT

Synthetic Image Generator Model:
Application of
View Angle Dependent Reflectivity Components
and
Performance Evaluation in the Visible Region

by
Richard B. Stark

February 1993

Proposal submitted to the Center for Imaging Science
in partial fulfillment of the requirement for the
Master of Science degree
at the
Rochester Institute of Technology

Adviser: John Schott, PhD

Committee Members: Mark Fairchild, PhD
Carl Salvaggio, MS

Proposal submitted to the Center for Imaging Science
in partial fulfillment of the requirement for the
Master of Science degree
at the
Rochester Institute of Technology


Synthetic Image Generator Model:

**Application of
View Angle Dependent Reflectivity Components
and
Performance Evaluation in the Visible Region**

Student Name Richard B. Stark

Social Security Number 092-60-4479

I have read and approved the thesis research proposal submitted by the above named student.

Signed:  Date 24 Feb 93
Primary Thesis Advisor *

Committee Members *John Schott, PhD

Mark Fairchild, PhD

Carl Salvaggio, MS

To be filed with appropriate graduate coordinator

Abstract

This proposal focuses on operation of the RIT Digital and Remote Sensing Lab's synthetic image generation (DIRSIG) software model within the 0.4 to 1.0 um wavelength region. The approach to this study is two-fold. First, an improved method is established for modeling reflectivity effects. This will include generating the associated reflectivity database. Currently, DIRSIG permits only ideal specular or ideal diffuse behavior. In a real scene, most objects actually exhibit some mixture of specular and diffuse behavior. The proposed treatment will essentially separate the reflectance characteristics into specular and diffuse components which vary as a function of view angle. Second, the performance of DIRSIG in the visible region using the improved technique must be evaluated. This will be accomplished by collecting truth data from an actual scene and comparing it to data from a synthetically generated image of the same scene. This evaluation will also serve as a first overall assessment of the model's performance in this wavelength region.

DRUG QUALITY INSPECTED 8

Accession For	
NTIS	CR-84
DTIC	145
Unannounced	15
Justification	
By	
Distribution	
Availability Codes	
Dist	Avail and/or Special
A-1	

Table of Contents

1. Introduction.....	1
2. Objectives.....	2
3. Background.....	5
3.1. Synthetic Image Generation Modeling.....	5
3.1.1. Applications.....	5
3.1.2. Modeling of Environment.....	6
3.1.3. Ray Tracing and Radiosity.....	8
3.2. Reflectivity Review.....	11
3.3. Reflectivity in Existing Visible SIG Models.....	15
3.4. Obtaining Reflectivity Values.....	18
3.4.1. Actual Measurements.....	18
3.4.2. Reflection Models.....	19
3.4.3. Hybrid Approach.....	22
3.5. DIRS Lab SIG.....	25
3.5.1. Scene Geometry Submodel.....	27
3.5.2. Ray Tracer Submodel.....	28
3.5.3. Radiometry Submodel.....	30
3.6. DIRSIG and Reflectivity.....	35
4. Approach.....	36
4.1. Modified Radiance Algorithm and Reflectivity Values...	36
4.1.1. Radiance Algorithm.....	36
4.1.2. Reflectivity Components.....	41
4.1.3. Generation of the Reflectivity Components.....	42
4.1.4. Validity of Reflectance Generation Method.....	46
4.2. Obtain Truth Data.....	48
4.2.1. The Scene.....	48
4.2.2. Image Collection.....	50
4.2.3. Associated Environmental Data.....	50
4.2.4. Equipment Calibration.....	52
4.3. Reflectance Measurements.....	53
4.4. Generation of Synthetic Images with Modified DIRSIG...	54
4.5. Evaluate Performance.....	55
5. Summary.....	59
6. Timetable.....	60
7. References.....	61

1. Introduction

This study focuses on operation of the RIT Digital and Remote Sensing Lab's synthetic image generation (DIRSIG) software model within the 0.4 to 1.0 μm wavelength region. DIRSIG is a robust model which generates a remotely viewed image by simulating the many interactions affecting energy reaching the sensor. The model provides for extensive treatment of the solar, atmospheric, target, and sensor interactions.

Evaluations of DIRSIG operating in the thermal (8-14 μm) and midwave (3-5 μm) infrared regions have been accomplished. These studies highlight potential problems with how well the model simulates radiance-surface interactions (reflectivity). These difficulties are hard to isolate in the midwave and thermal IR regions due to the complicating presence of surface emissions. Therefore, improvements should be made and assessed by operation in the visible region, where surface emissions do not exist. This study is intended to set the groundwork for future enhancements in this area.

Currently, DIRSIG only allows for ideal specular or ideal diffuse reflectance behavior. In reality, most objects exhibit some mixture of specular and diffuse characteristics which are dependent on scene geometry. To improve DIRSIG, the treatment of reflectance should account for the effects of scene geometry dependent, specular and diffuse components. Much difficulty lies with actually acquiring the values of the reflectivity components. Many models have been developed over the years to describe reflectivity. Unfortunately,

the literature doesn't contain any reflectance models that describe the reflectivity as required by DIRSIG. DIRSIG's rendering technique, as currently stands, requires view angle dependent components used to modify ideal radiance-scene interactions.

The approach to this study is two-fold. First, an improved method is established for modeling reflectivity effects. This will include generating the associated reflectivity component database. The reflectivity components will be determined by a practical approximation method based on the established models. Second, the performance of DIRSIG in the visible region using the improved technique must be evaluated. This will be accomplished by collecting truth data from an actual scene and comparing it to data from a synthetically generated image of the same scene. This evaluation will also serve as a first overall assessment of the model's performance in this wavelength region.

2. Objectives

The overall objectives of this thesis are to modify the DIRSIG treatment of reflectivity and evaluate DIRSIG's performance in the visible spectrum. As mentioned, DIRSIG was developed for operation in the infrared region and therefore no visible region baseline exists to compare the effects of modifications.

The hypothesis is that the modifications will result in realistic radiance-surface interactions within the scene and that any significant errors will be attributable to other aspects of the model.

The following will be accomplished to meet the objectives:

First. Apply a modification to DIRSIG which provides a more realistic treatment of reflectivity. This includes a method of generating the required material type reflectivity values. The DIRSIG modification, described in the approach section, is based on a combination of theory and laboratory measurements.

Second. Obtain ground truth data by imaging an actual scene from a fixed view angle with various solar illumination angles. This entails establishing the actual scene, collecting the images, measuring atmospheric effects, monitoring the environment, and performing equipment calibrations.

Third. Generate material type reflectivity values required by the modified DIRSIG algorithm to allow creation of synthetic images. This includes laboratory measurements of truth scene samples.

Fourth. Generate selected images of the ground truth scene using the modified DIRSIG model.

Fifth. Evaluate the performance of the modified DIRSIG model by comparing the generated images against the observed truth data. Explore reasons for discrepancies by assessing inherent errors within the overall DIRSIG model and the reflectivity component characterizations. In light of performance and error assessment results, discuss the value of various engineering trade-offs used within DIRSIG. Finally, recommend where efforts should be focused to further improve the quality of visible image generation.

3. Background

3.1 Synthetic Image Generation Modeling

Today's information dependent society increasingly craves imagery for many different applications. A major category of imagery is of outdoor scenes recorded by a remote sensor. Under some circumstances, it may be prohibitive to record the image of an actual scene. Whether the prohibition is levied by money, time, or accessibility constraints, there is a great need for the ability to simulate realistic images. The creation of realistic artificial images using detailed computer software algorithms, is referred to as synthetic image generation (SIG). The degree of realism required of SIG varies with the particular application of the imagery. For instance, some applications may only require accurate spatial information, while others may require accurate spatial and radiometric detail.

3.1.1. Applications

Raqueno, et al (1991) describes various applications appropriate for SIG techniques. One example is resource management, where images from remote sensors are used to assess a particular phenomenon occurring over large areas. Simulations can be used to 'pre-fly' a target to determine the best geometry and environmental conditions for observing the phenomenon of interest. The actual collection can then concentrate on a few designated "flights" to record the desired information, saving both time and money.

Another application is training for image exploitation. From

the tedious human assessment of detailed reconnaissance images to the high speed machine interpretations of terrain following radar, image exploitation techniques involve applying decision algorithms to assess image characteristics. Training or evaluating both human and automated analysts is limited by the availability of imagery incorporating desired combinations of sensing geometry and environmental conditions. Synthetic images can be used to depict scenes normally restricted to actual collection and depict them under various conditions. Therefore humans and machines can be presented images which provide the needed challenge to their respective capabilities.

3.1.2. Modeling of Environment

To create realistic synthetic images, all potential sources of energy that may be directed into a sensor must be modeled. Of this energy, only the region of the electromagnetic spectrum that can be detected by a particular sensor must be accounted for. Even though SIG techniques are useful for a variety of sensors sensitive to all wavelengths, much of the related research focuses on electro-optical applications in the 0.4 to 15.0 μm region. The primary energy sources within this region are solar and thermal emission.

As these energies propagate, they are potentially modified by atmospheric and/or surface interactions. The extent of effects depend on the relation between the wavelength of the energy and molecular particle size making up the atmosphere or surface it interacts with. As the molecular content of the atmosphere changes,

so does the degree of scattering and absorption of radiation. The surface interaction with energy is of primary interest because understanding this provides an opportunity for exploitation. (Lillisand and Kiefer, 1987).

According to the principle of conservation of energy, incident energy onto a surface must either be absorbed, reflected, or allowed to transmit. Since transmission is not a factor for the solid surfaces of interest within a typical scene, the only options are either reflection or absorption. Absorption is proportional to emission if the surface is in thermal equilibrium with its surroundings. Generally, the predominant surface interaction for incident energy below 3 μm is reflection. For longer wavelengths, the predominant effect is absorption/emission (Lillisand and Kiefer).

Figure 3.1 displays the various energy interactions occurring within a given scene. A scene will normally consist of solar energy reflected from the surface, thermal energy emitted by the surface, atmospheric downwelling energy, and atmospheric upwelling energy. The upwelling and downwelling energy are a result of the atmosphere's molecules scattering and emitting energy.

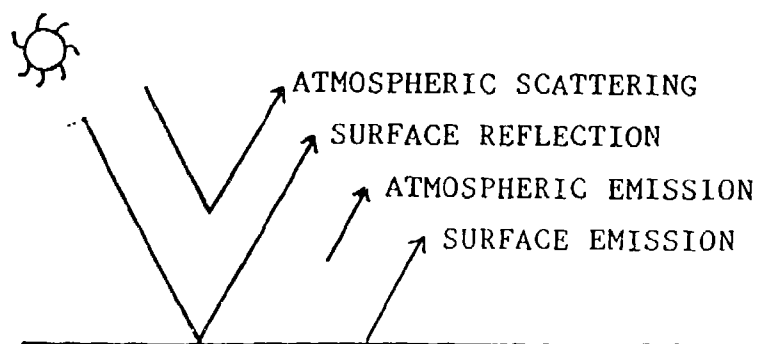


Figure 3.1 Energy interactions within a scene

The bulk of published work regarding operating SIG models focuses on the thermal infrared region (8 - 15 μm) in support of research on infrared sensors for defense and resource management applications. Within this region the solar surface reflection is vanishingly small compared to surface emission. Some SIG models will also operate within the midwave IR region (3-5 μm) where both surface reflection and emission are equally important. However, these simulations are usually restricted to night to avoid the solar reflection effects. Raqueno, *et al* provides a good review of existing IR based models.

This proposal focuses on the 0.4 - 1.0 μm range. This region will be referred to as the visible region, even though the human eye is only sensitive 0.4 - 0.7 μm . The sensitivity region of many silicon based charged couple device (CCD) sensors is defined by this wider range. Within the visible spectrum atmospheric effects and surface absorption are minor. Therefore, reflectivity is the primary source of energy interaction and effective visible SIG modeling is dependent on proper treatment of its effects.

3.1.3 Ray Tracing and Radiosity

Prior to reviewing reflectivity, a brief look is made of how many SIG models account for the interaction of energies within a scene. Comprehensive treatments of energy propagation are generally complex, cumbersome algorithms created for theoretical purposes and not meant for practical use. Therefore, early SIG models relied on relatively simplistic methods. However, with dramatic increases in computer processing power in the 1980's, development efforts have

focused on providing practical methods of applying complex theoretical energy propagation algorithms. Two such methods are ray tracing and radiosity (Goral, et al, 1984).

Ray tracing is a backward reconstruction process that determines the energy reaching a sensor's pixels by casting rays into the scene and "back tracking" until all energy sources are accounted for. In the simplest case, a ray that encounters an object is redirected by a mirror-like reflection. Figure 3.2 shows a few simple rays. This method is restricted in that it employs point sampling of energy contributions along the ray. Outside the ray vector, the energy contributions are approximated by constant ambient terms. This results in some loss of differential energy source information which may result in inability to adequately simulate detail within areas such as shadows. A complete discussion of ray tracing is presented by Bouville and Bouatouch (1991).

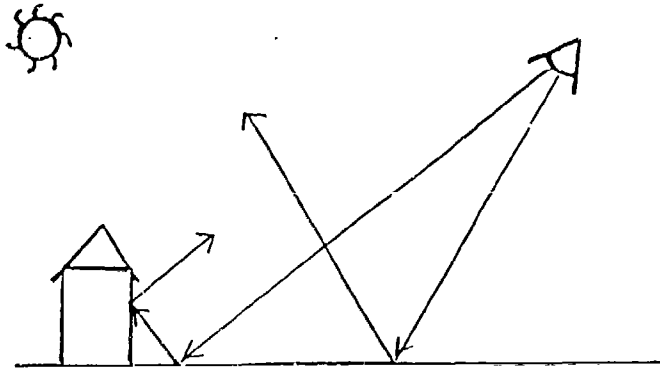


Figure 3.2 Sample rays within ray tracing

Radiosity is a method which decouples the calculation of energy leaving the surfaces within a scene and the propagation of the

energies to the sensor. First, the energy leaving the surfaces for the entire scene are determined through illumination and reflectance calculations. All objects are considered diffuse and inter-object illumination is determined by geometric relations between the objects. After this, the energy reaching the sensor is assessed from any particular view angle. The appeal of this process is that the "...environmental intensity information can be preprocessed and subsequently used for multiple views." However, due to this large preprocessing cost, radiosity is limited to static scenes. Also, only diffuse scenes can be generated and the final image is only as accurate as the degree of discretization within the scene model. (Greenberg, 1989).

Since this study is concerned with practical application of both specular and diffuse reflectivity characteristics, direct ray tracing approaches will be emphasized.

3.2 Reflectivity Review

In general, reflectivity is the scattering phenomenon of incident energy by a surface. Different terms are used to describe the relation between incident and reflected light. Uniformly incident energy is defined as the *incident irradiance (E_i)* with units of Watts per meters². The radially reflected energy from a point on the surface will propagate over a range of angles and is defined as the *reflected radiance (L_r)* with units of Watts per meters² per steradian (Nicodemus, 1965). These terms are depicted in figure 3.3. The surface characterization relating the reflected energy into the entire hemisphere to the total incident energy is defined as the *Reflectance (R)* and has no units (Lillisand and Kiefer). For most surfaces, reflection will attenuate the energy due to absorption.

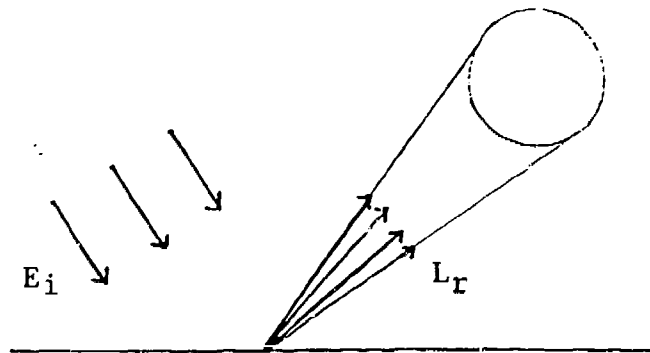


Figure 3.3 Incident irradiance (E_i) and reflected radiance (L_r)

An intuitive characteristic of reflectivity is that it varies as a function of incident and viewing angles. According to Schott, et al (1990), "data acquired at fixed illumination angles indicate that common backgrounds can vary in their reflectance factors by 100 to 400 % for view angles ranging from nadir to 75 degrees off nadir."

For most modeling applications, the geometrical dependence of the reflectance is an important consideration and therefore the basic definition of reflectance is usually insufficient. Feng, et al (1992), characterizes this geometric reflection phenomenon as the *Bidirectional Reflectance Distribution Function (BRDF)*. BRDF is defined as the ratio of the reflected radiance to the incident irradiance within a small solid angle. This relation is depicted in equation 3.1 and figure 3.4.

$$BRDF = (L_r) / (L_i \cos\theta_i d\omega_i) = L_r / E_i \quad (3.1)$$

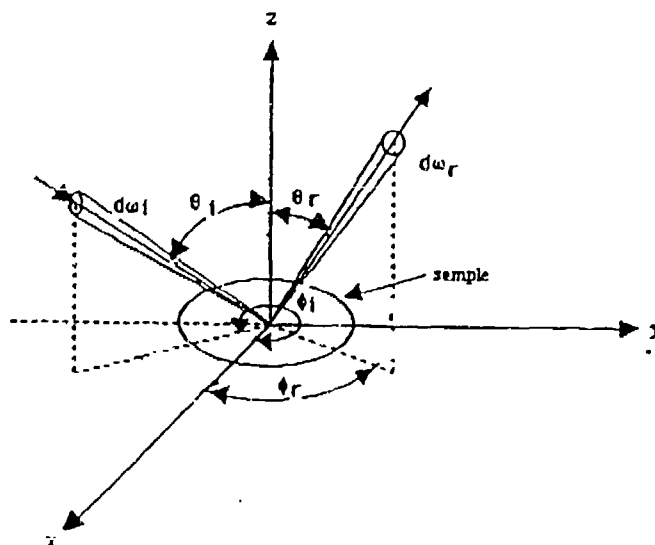


figure 3.4 Geometric relations of BRDF

To characterize a surface's BRDF at a particular geometry, both the incident irradiance and reflected radiances would need to be known. These values are difficult to measure simultaneously with a typical laboratory set-up. Therefore another quantity is often used to characterize a surface reflectivity. This is the *bidirectional reflectance factor (BDRF)*. The BDRF is the

"ratio of the radiant flux actually reflected by a sample surface to that which would be reflected into the same reflected beam geometry by an ideal (lossless) perfectly diffuse (Lambertian) standard surface irradiated in exactly the same way as the sample." This unitless value is closely related to the BRDF as shown in equation 3.2 (Feng, et al, 1992).

$$\text{BDRF} = \pi \text{ BRDF} \quad (3.2)$$

The previous characterizations are very specific for a particular surface in describing the "amount" of energy reflected. Two other descriptions provide a more qualitative description of the "dispersive" behavior of reflectivity. When reflected energy is concentrated at an angle equal to the angle of incidence, but 180 azimuthal degrees away, it is referred to as *specular reflection*. An ideal specular surface has a BRDF which is a delta function at the reflection angle, and zero everywhere else. *Diffuse reflection* is when the reflected energy is spread in all directions. The BRDF of an ideal diffuse surface is equal at all view angles as described by Lambert's law. Such a surface is also referred to as Lambertian. (Sillion, et al, 1991).

In most real, nonideal surfaces, the dispersive behavior will be a mixture of both specular and diffuse characteristics. As shown in figure 3.5, the energy will reflect in all directions, but will build up a concentration in the specular direction. The degree of concentration will characterize surfaces as either more specular or more diffuse in behavior. Torrence and Sparrow (1967) have shown

that in some instances, "...a maximum in the distribution of the reflected radiance occurs at an angle larger than the specular angle." This off-specular peak has been observed in surfaces whose RMS surface roughness is comparable to (or greater than) the incident energy wavelength.

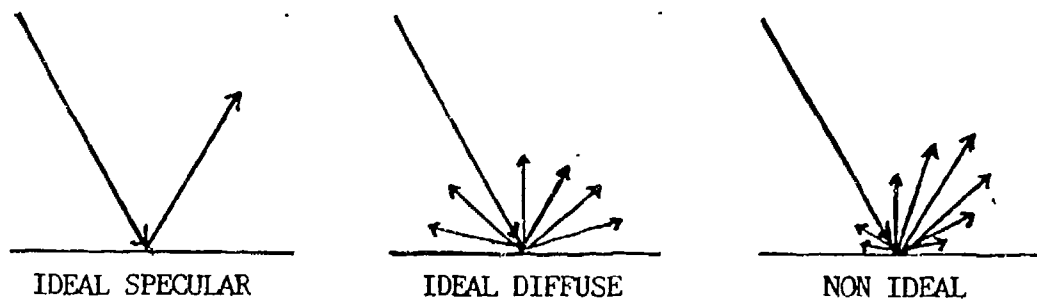


Figure 3.5 Reflectivity Characteristics

3.3 Reflectivity in Existing Visible SIG Models

The majority of computer graphics literature discuss algorithms that forgo proper radiometry. Those concerned with realism care more about if the overall image simply appears correct, which can be accomplished by various empirical methods. In fact, only four operating SIG models were found to be concerned with creating realistic, radiometrically correct images in the visible region. Of these, all but one are infrared models that have been "extended" to operate in the visible. The fundamental algorithms for these models were probably designed to describe the nuances of thermal emissions as opposed to those of solar reflections.

This section provides a brief overview of how these visible SIG models treat surface reflection. The models are used in a variety of applications whose requirements range from simple reflection approximations to detailed characterizations. In general, the more detailed models are slower to implement and require much more knowledge of the object surfaces. The trade-offs must be considered when rating the value of different SIG models and their surface reflectance treatments. Both the application and general description of reflection treatment is provided here.

Two "crude" treatments of surface reflectance are found in SIGs developed by Texas Instruments and Photon Research. The *Texas Instrument* application generates synthetic images to create a database for testing automatic target recognition algorithms. These algorithms primarily seek to make decisions based on the general categorization of scene objects as distinguished from background.

This categorization is mostly spatial with relative contrasts needed to further discern relative objects. The general nature of the Texas Instrument SIG model requires only a simple approximation of surface reflection. Therefore all objects are simply assumed to be diffuse and total diffuse reflectance values are used (Lindahl, et al, 1990).

The SIG model implemented by *Photon Research* generates high altitude earth background imagery and also requires only a simple approach to surface reflectance. This model also uses a diffuse reflectance value to determine the surface effects within a scene. Justification for the simplistic approach is due to the high altitude nature of the imagery which reduces the resolution. Within the large ground sample spot size, the natural objects vary quite a bit and obtaining actual reflectance values would be futile (Reeves, et al, 1988).

The visible SIG model developed by the *Georgia Tech Research Institute* generates more detailed images. A rendering method called environment mapping is used which is described as a cross between radiosity and ray tracing. As in radiosity, the energy leaving the surfaces for the entire scene are precalculated. However, six different geometrical arrangements are considered, each using a common specular reflectance value. These represent the energies leaving the surface due to specular reflectivity. The energy leaving the surface due to diffuse reflectivity are found by simply averaging the six specular values. Final rendering is accomplished using ray tracing techniques that interrogate the scene and apply the appropriate specular reflected energy value plus the diffuse

reflected energy. Thus only one reflectance value (which is specular) is used for a particular surface (Cathcart, et al, 1990).

A visible SIG model that is based on a detailed characterization of reflectivity exists within the *Computer Graphics Program at Cornell University*. The reflectance model is an in-depth physics based algorithm that has evolved over the past twenty years and incorporates full BRDF effects. This model is referenced by most other journal articles found relating to visible SIG and reflectance theory. An important aspect of Cornell's SIG model is that it employs a combination of ray tracing and radiosity rendering methods to capture the benefits of both techniques (Wallace, et al, 1987).

There are some limitations of the Cornell SIG model. The detailed reflectance model may actually be too complex for many practical applications. Also, the radiometry algorithm which governs the ray tracing and radiosity does not incorporate many atmospheric effects on a scene. It is these reasons that the Cornell SIG model is primarily used to image scenes with highly controlled environments which have a minimum number of objects and no atmospheric elements to contend with (i.e. the production of quality indoor images of simple objects). Such restrictions make the Cornell model unattractive for synthetically generating remotely sensed images.

3.4 Obtaining Reflectivity Values

An important part of SIG is actually obtaining the reflectance values for a particular surface and various techniques exist to generate this data. The most straight forward way is to actually measure the complete set of BRDFs (or BDRFs). On the other extreme, detailed, theoretically based, reflectivity models can be used. A third method is to use a hybrid approach of actually measuring a representative subset of reflectance values and then applying a model which generates all other values of interest. The appropriate technique to apply is one that balances out the required realism and the need for a practical process. These three methods will be discussed in this section.

3.4.1 Actual Measurements

Actually measuring BDRF values for a surface should provide the most exact representation of reflectance. Feng (1990) describes how this data is obtained by systematically measuring the reflectance at various illumination and viewing angles throughout the hemisphere. However, there are trade-offs to consider when acquiring this degree of precision.

First of all, the apparatus required to precisely measure the BDRF is complex and expensive. This equipment must be capable of adjusting the source, sensor and sample to emulate all possible geometrical configurations. The entire system must be extremely stable over the long period of time required for measurement. Also, the sensor must be spectrally sensitive to adequately measure over

the wavelength bands desired.

Additionally, a major impediment for practical measurement of complete BDRF values is the large amount of data generated. Even if the discrete measurements were spatially "spread out" and then interpolated, the amount of data is enormous. For example, for only one sample, if only five illumination angles were used, along with 15 view angles, nine azimuthal angles, and three spectral bands, the number of measurements would equal $5 \times 15 \times 9 \times 3 = 2,025$.

If resources were available for purchasing the necessary equipment and then creating a fairly automated method of using it, this method may be most appropriate for generating reflectance data. However, for remote sensing applications, samples cannot be acquired for all surfaces in the scene. The actual scene may be in a restricted area or the scene may contain living surfaces such as plant life whose reflective properties will change after removal. Therefore many surface reflectances still need to be approximated based on *similar* materials used in laboratory measurements. In many instances this may indeed neutralize any original benefits.

3.4.2. Reflection Models

Use of models to predict reflectance values requires a thorough understanding of actual surface characteristics. There are many models available with varying levels of complexity. Like choice of overall SIG model, the choice of reflectance model depends on the degree of accuracy required for the application.

Early reflection models simply treated all surfaces as diffuse.

However in 1975, Phong introduced a more realistic model to account for the fact that more light is reflected in the specular direction. This was accomplished by adding a specular reflection component (R_s) to the simple diffuse component (R_d).

$$R = R_d + R_s \quad (3.3)$$

For a mirror surface, this added component would only be found where the scene geometry was such that the view angle *equaled* a source's incident angle. Phong realized that most surfaces were not mirrors and the specular component is more of a lobe which "falls-off" at varying rates. He incorporated these lobe effects by modifying the specular component with the cosine of the surface normal (N) and the vector (H) bisecting the illumination-view angle (See figure 3.6). To allow further empirical modification of the specularity, Phong suggests taking this cosine function to some power (Magenat-Thalman and Thalman, 1987).

$$R_s' = R_s (\cos \alpha)^n \quad (3.4)$$

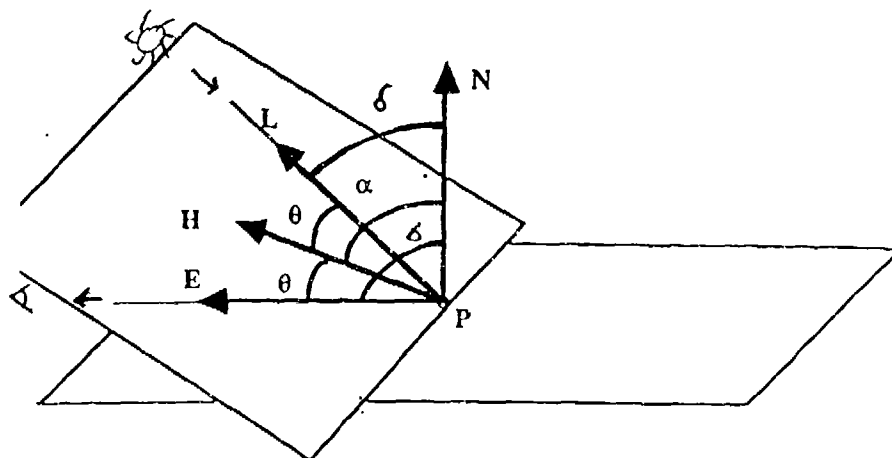


figure 3.6 Phong model geometry

While the Phong reflectance model is more accurate, it is still heavily empirical. Blinn (1977) sought to overcome this by using the less empirical Torrance-Sparrow model for the specular reflectance component (R_s). While Phong treats the surface as a plane whose orientation effected the specularity, the Torrance-Sparrow model assumes the surface is itself a collection of small mirror like facets. The specularity of the surface results from the orientation of the the facets.

$$R_s = (D G F) / (\cos \sigma) \quad (3.5)$$

- where:
- D represents the distribution function of the facet normals which is statistically derived
 - G is the attenuation due to shadowing and obscuration(function of roughness parameters)
 - F is the Fresnel factor of the surface, a function of index of refraction
 - σ is the angle between the surface normal (N) and the viewing direction (E), see figure 3.6

As mentioned earlier, a complex reflectance model was developed at Cornell University by Cook and Torrance (1982). This heavily theoretical model incorporates BRDF effects and still allows for overt empirical adjustment. The adjustment is provided by characterizing a surface with percentages of specularity (s) and diffuseness (d).

$$R = d R_d + s R_s, \quad \text{where } s + d = 1 \quad (3.6)$$

The BRDF effects are incorporated into the specular component by accounting for the solid angle (π) defined by the sensor and the illumination angle (δ) shown in figure 3.6.

$$R_s = (D G F) / \pi(\cos \sigma)(\cos \delta) \quad (3.7)$$

Also at Cornell, He, *et al* (1991) introduced a more accurate model for reflectance based on physical optics. This model has a third term that represents the spread and direction of the specular lobe, as Phong tried to do empirically. This term is referred to as the directional diffuse component (Rdd). These components are displayed in figure 3.7.

$$R = R_s + R_d + R_{dd} \quad (3.8)$$

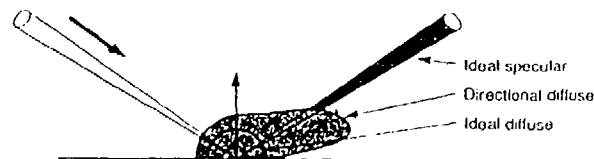


figure 3.7 He, *et al*, light intensity distribution

Determining values for these terms require extensive calculations and knowledge of such surface characteristic parameters as polarization effects, complex index of refraction, RMS roughness, and autocorrelation length. These components are fully derived in the referenced journal article.

3.4.3. Hybrid Approach

Another method, developed by the Environmental Research Institute of Michigan (ERIM), generates reflectivity values by incorporating both measurements and modeling. In brief, the ERIM method requires a small subset of BRDF data for a particular surface. The BRDF for any geometric situation is calculated from a theoretical reflection model using the BRDF subset and known surface parameters. This reflectance model is very similar, although less complex, to

that of He, et al. Particular BRDF values can be found without having to measure and store large volumes of data or without having the long processing time required for complex theoretical models (ERIM BRL Report, 1974).

As mentioned, the ERIM reflectance model is very similar to the models developed at Cornell. Like the Cook and Torrence model, it consists of two components, surface (specular) and volumetric (diffuse). Also, similar to the He, et al model, the volumetric component is broken into Lambertian (ideally diffuse) and non-Lambertian (directional diffuse). Furthermore, the model accounts for the reflective dependency on polarization.

The actual subset of reflectance data used by the model components is referred to as "zero bistatic" reflectance values. Zero bistatic refers to the source-sensor angle being held near zero. As shown in figure 3.8, the vector representing the source-sensor location is at an angle θ_n from nadir. This angle is incremented from 0 to 90 degrees and BRDF values are recorded at each step. The scan is performed twice. First, with the sensor and source at the same polarization and then with sensor and source cross polarized.

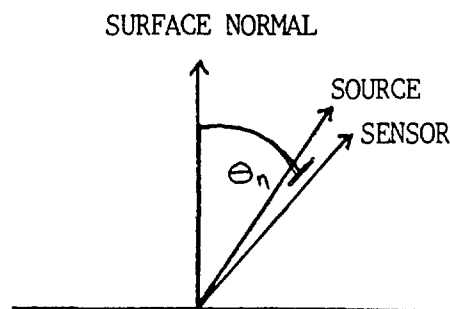


figure 3.8 Zero bistatic measurement geometry

The surface component consists of variables similar to Cornell's specular component. The main difference is the distribution of facet normals for a particular geometry is represented by the difference of the two measured bistatic values further modified by cosine factors. The Lambertian volume component is similar to Cornell's ideal diffuse component in that a single value is used for all geometries. It is calculated by doubling the cross polarized zero bistatic value at nadir, which is measured in only one polarization. The non-Lambertian volume component is similar to Cornell's directional diffuse. The height of the nadir peak of a material's cross polarized bistatic scan is used to calculate this component value.

All three techniques for generating BRDF values share a common problem. They all rely on a material data base that may be difficult to sufficiently populate. Furthermore, the material you are assessing must be represented. Otherwise, the values for a similar material will be used and any gains made by using these detailed approaches may be lost.

This study develops a practical approach to generating reflectivity values based on a simplified hybrid method. The actual measurements will require quick, straight-forward, goniometric scans. Deriving the appropriate reflectance values from the measurements will be accomplished by emphasizing various segments of the data. The theory behind this treatment incorporates many of the important aspects found in all three techniques described above. Furthermore, this approach is concerned with incorporating only those reflectivity characteristics actually exploited by the SIG model.

3.5 DIRS Lab SIG

This study will focus on modifying an existing infrared SIG model to operate in the visible (0.4 -1.0 μm) region to incorporate some of the reflectance concerns discussed thus far. This SIG model, described in detail by Raqueno, et al (1991), was developed by the Rochester Institute of Technology's Digital Image and Remote Sensing (DIRS) Lab and is referred to as DIRSIG. DIRSIG provides extensive treatment of the solar, atmospheric, scene object, and sensor effects for remotely sensed images.

The DIRSIG model consists of the following five submodels: scene geometry, ray tracer, temperature generator, radiometry, and sensor. Relevant scene input data include materials, weather, and atmosphere. The submodels interact to create the final synthetic image as shown in figure 3.9. Since this study evaluates only the radiance reaching the "front end" of the sensor and is restricted to the visible region, the sensor and temperature generator submodels will not be discussed. A description will be given to the applicable portions of the scene geometry, ray tracer, and radiometry submodels. Greater detail on the submodels can be found in the referenced document.

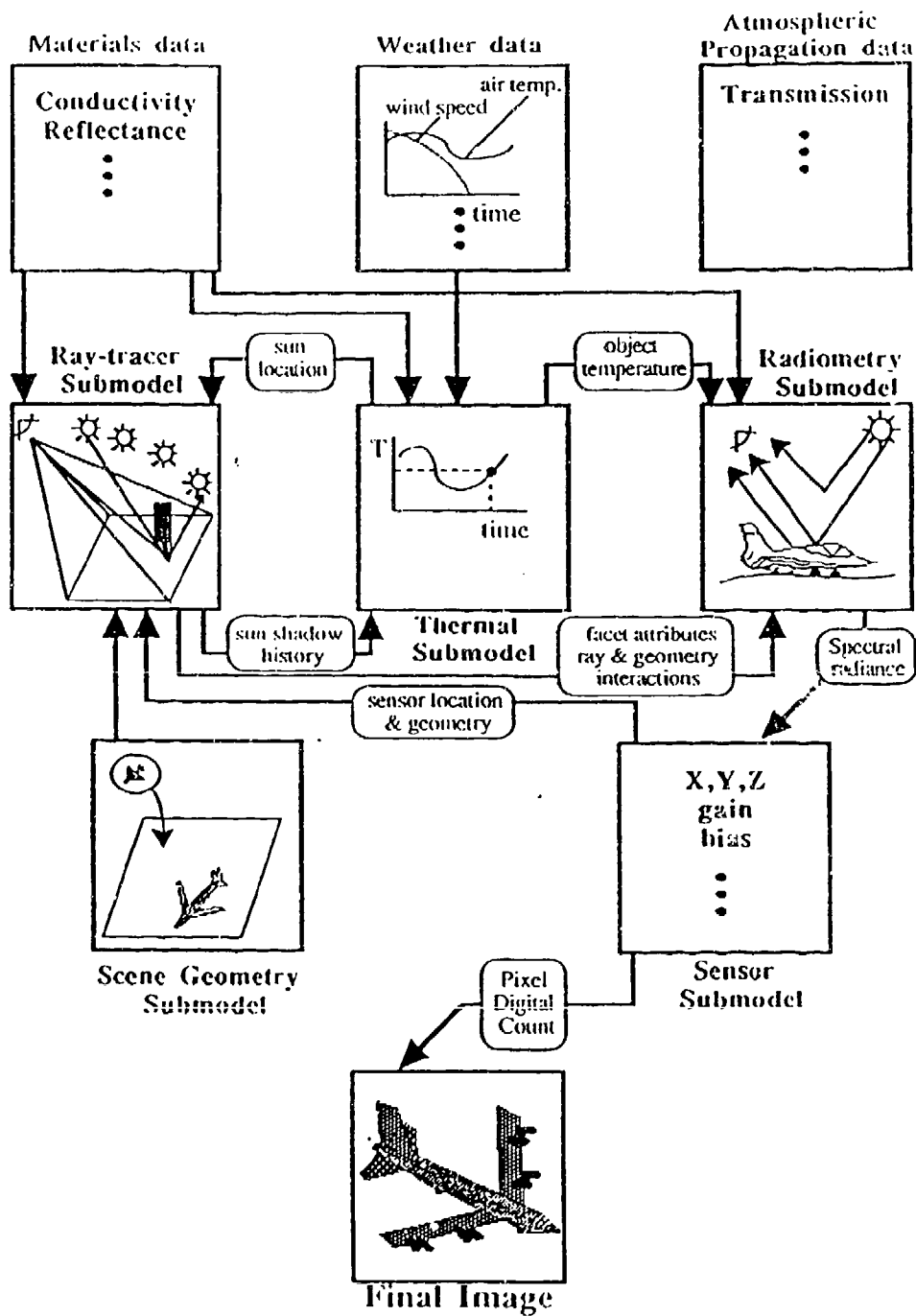


figure 3.9 Submodel interactions within DIRSIG

3.5.1. Scene Geometry Submodel

The starting point for generating a synthetic image is the scene geometry. This submodel uses a 3-D AutoCad model of the objects, along with scaling and orientation algorithms, to create the desired scene. The scene objects are subdivided into facets which make-up the most basic element. Each facet is described by pointers to three nodes (geometry, orientation, and attribute) which serve to link the various properties designated by the model builder.

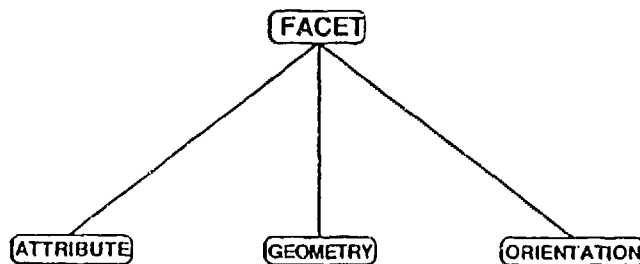


figure 3.10 Facet Subnodes

The geometry node defines the coordinates of the facet's points as well as the normal vector from the facet plane. The orientation node provides angle information regarding the orientation of the facet normal with respect to the earth and sun. These two nodes provide the data needed to trace the basic interaction of a propagated ray. The attribute node contains additional parameters that define the facet's physical properties (see figure 3.11). The primary property for this study is the material code, which points to a common materials database that can be accessed by any facet. Figure 3.12 displays the types of information that can be assigned to this database for use by the overall SIG process. It is this database that will contain the generated reflectance values that determine the result of light-surface interactions.

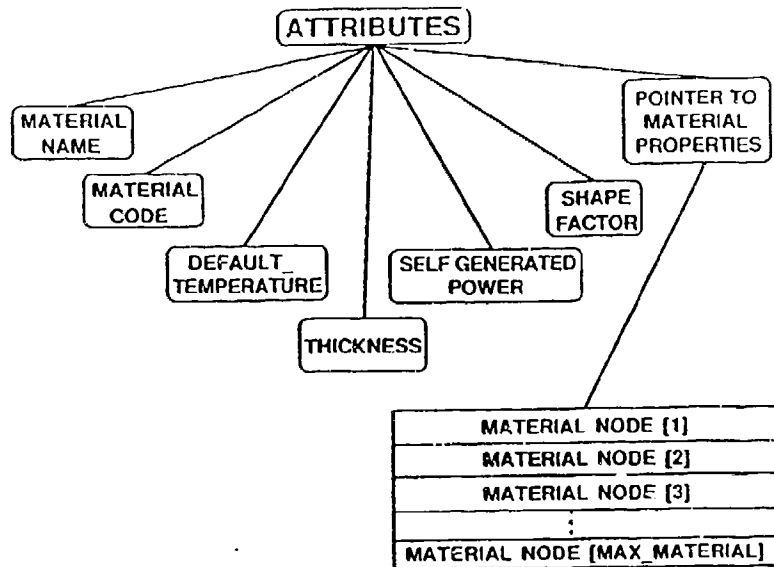


figure 3.11 Attribute Subnodes

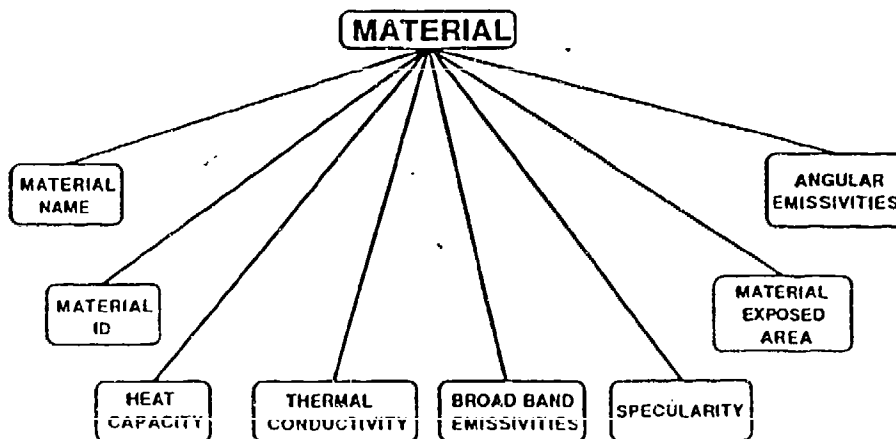


figure 3.12 Material Subnodes

3.5.2. Ray Tracer Submodel

The ray tracer submodel is tasked with retracing the paths of photons reaching each sensor picture element into the scene itself. This allows for proper calculation of the radiance based on the originating source and intervening scene interactions such as

atmospheric absorption and material reflection. To perform this task, the submodel also serves to coordinate the entire simulation process.

For an ideal tracing, each time a ray interacts with a facet, secondary rays would need to be sent out in *all* directions. Each secondary ray would determine the incoming energy to the facet from a particular direction. The energy from each direction would then be attenuated by a specific BRDF value based on the orientation of the primary ray and each secondary ray. This ideal assessment of the incident energy is depicted in figure 3.13.

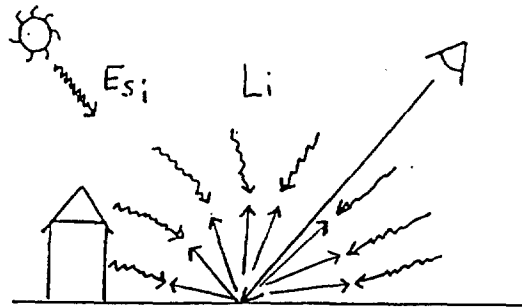
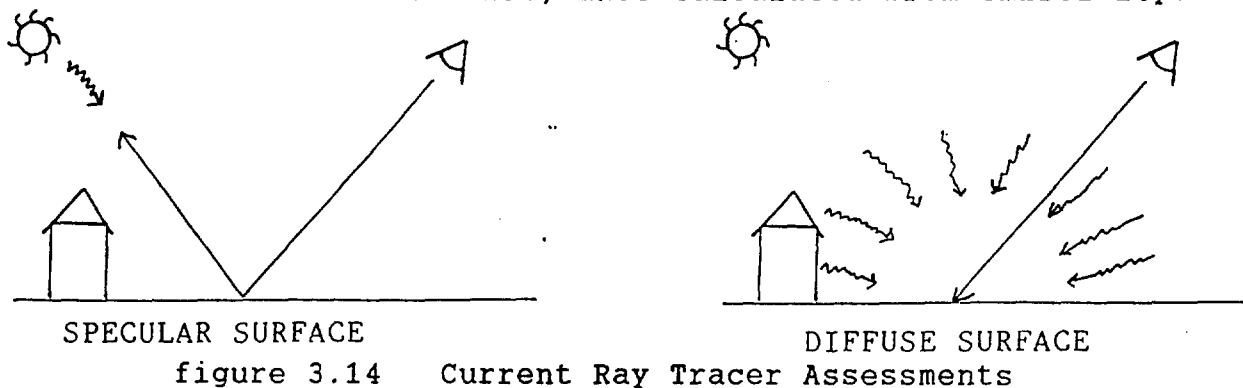


figure 3.13 Ideal Ray Tracer Assessments

Although such an ideal scheme is feasible, there are reasons why it is not practical. First, generating all the specific BRDF values would require many resources as discussed in section 3.4. Thus, it is unlikely that a materials database would ever be sufficiently populated. Second, to fully exploit such BRDF phenomenon as sharp specular peaks, a high density of secondary rays are required to provide sufficient angular resolution. Assessing a high enough density of secondary rays will be similar to integrating the incident energy over the hemisphere, as shown in equation 3.9. Such a large volume of primary rays may result in prohibitive processing time.

$$L_r = (E_{si}) (BRDF) + \int L_i d\omega_i BRDF \quad (3.9)$$

For practicality reasons, the current approach by DIRSIG avoids complete sets of secondary rays for each facet interaction by assuming each material is either completely specular or completely diffuse. If a surface is labelled as specular, then a secondary ray is cast at the "specular" angle and assessed for incoming energy content. If the surface is labelled as diffuse, then no secondary rays are traced and the incoming energy is assessed from the hemispheric downwelled radiance, effective solar radiance, and applicable background radiances. These are depicted in figure 3.14. The incoming energy in the specular case is modified by a view angle dependant reflectance value, calculated from an angular emissivity value. For the diffuse case, the incoming energy is modified by a total diffuse reflectance value, also calculated from emissivity.



For the longwave infrared region, it has been determined by Shor (Raqueno, et al, 1991) that the maximum "depth" of ray-facet interactions to be traced is two. Computations of rays beyond this result in insignificant radiance contributions. No similar testing has been done in the midwave infrared and visible regions, but the same results will be assumed.

3.5.3. Radiometry Submodel

The radiometry submodel actually calculates the radiance reaching the front end of the sensor according to the interactions described by the scene geometry and ray tracer submodels. The ray-facet interactions are governed by the material characteristics database. The ray-atmosphere interactions are provided by an algorithm referred to as the spectral vector generation model (SVGM) which was developed by Salvaggio, et al (1991).

SVGM is a modified version of another algorithm called LOWTRAN, developed by the Air Force Geophysics Laboratory. "LOWTRAN models the atmosphere as many individual layers, each of which exhibits either pre-defined or user-specified meteorological conditions, atmospheric composition of gases, aerosol type and specific scattering phase functions, as well as sensitivity to global position" (Raqueno, et al). The modified model provides DIRSIG with such parameters as exoatmospheric solar irradiance, atmospheric transmission, and downwelling sky radiance.

The SIG algorithms required to determine the radiance reaching the sensor for each ray cast are straight forward. If the ray's primary target is diffuse, the radiance is determined from an ideal diffuse treatment using equation 3.10. If the ray's primary target is considered specular, the radiance is found from an ideal specular treatment using equation 3.11. In each case, the total radiance reaching the sensor for any primary ray is found by adding the atmospheric upwelled radiance. To further limit the extent of the calculations, the background objects are always considered diffuse.

The parameters required by these equations are either defined by the material database, generated by another submodel, or calculated by the SVGM. Table 1 provides definitions of these parameters. Figure 3.15 illustrates the angles used in the equations. Figure 3.14 displays the four general interactions incurred by the ray tracer in implementing the radiometry algorithm.

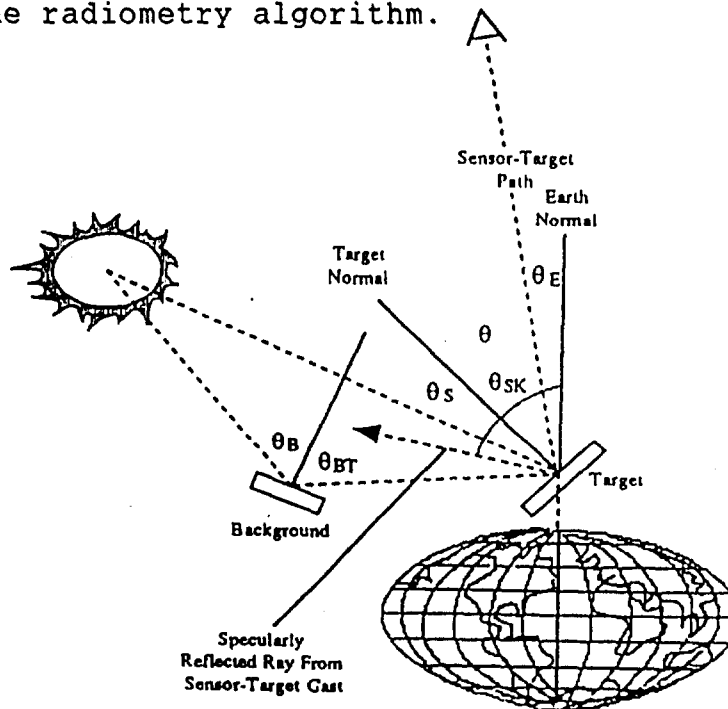


figure 3.15 Angles in radiometric equations

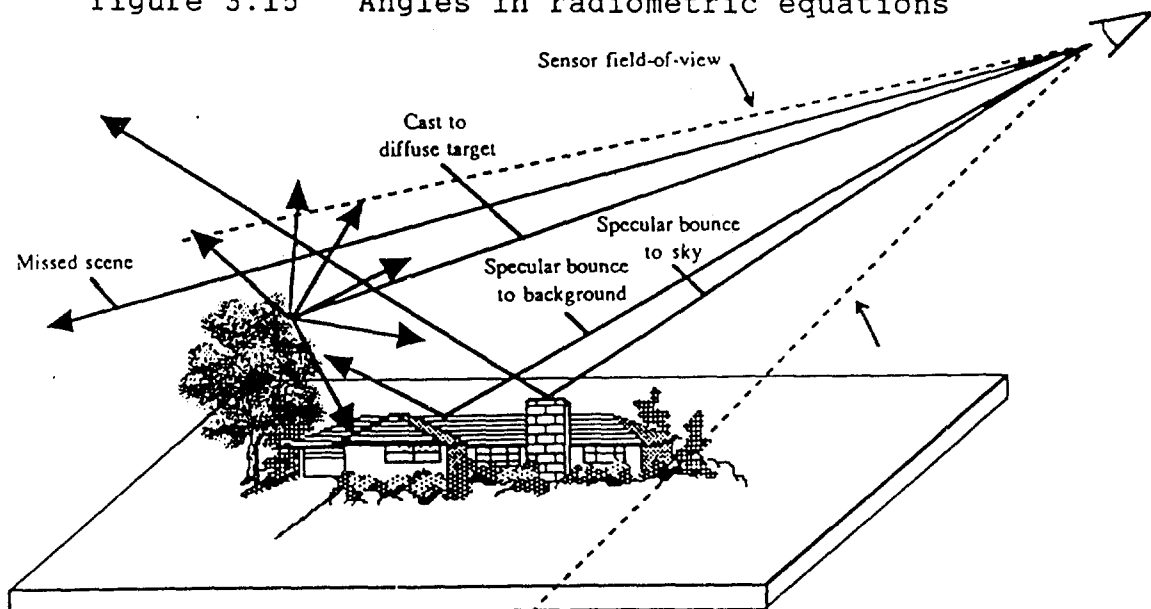


figure 3.16 Four general ray tracer interactions

Diffuse Objects:

$L = \text{Diffuse Component} + \text{Upwelled Component}$

$= (\text{solar} + \text{downwelled} + \text{background}) (\text{diffuse reflectance}) (\text{atm transmission}) + \text{upwelled radiance}$

$$= \left[(E_s/\pi) I_t \tau_1 \cos\theta_s + F L_{\text{dsky}} + (1-F) \left((E_s/\pi) I_b \tau_1 \cos\theta_b + F L_{\text{dsky}} \right) R_b(30^\circ) \right] R(0^\circ) \tau_2(\theta_E) + L_u(\theta_v) \quad (3.10)$$

Specular Objects:

$L = \text{Specular Component} + \text{Upwelled Component}$

$= (\text{solar} + \text{downwelled} + \text{background}) (\text{specular reflectance}) (\text{atm transmission}) + \text{upwelled radiance}$

$$= \left[(E_s/\pi) I_t \tau_1 \cos\theta_s + L_d(\theta_{\text{sky}}) \tau_{\text{bsp}} + (E_s/\pi) I_b \tau_1 \cos\theta_b R_b(\theta_{\text{bt}}) (1 - \tau_{\text{bsp}}) \right] R(\theta_v) \tau_2(\theta_E) + L_u(\theta_v) \quad (3.11)$$

$R(\theta_v)$	target reflectance , calculated from $1-\epsilon(\theta_v)$
R_b	background reflectance
L	spectral radiance reaching front of the sensor
L_{dsky}	downwelled spectral radiance due to scattering integrated over the skydome
$L_d(\theta_{sky})$	directional downwelled spectral radiance due to scattering
$L_u(\theta_v)$	upwelled spectral radiance due to scattering along the target-sensor path
E_s/π	exoatmospheric solar spectral radiance
τ_1	atmospheric spectral transmission along the source - target path
$\tau_2(\theta_v)$	atmospheric spectral transmission along the target-sensor path
τ_{bsp}	transmission of an object in the target-sky specular bounce direction
I_t	target sun/shadow flag (1 or 0)
I_b	background sun/shadow flag (1 or 0)
F	shape factor, the fraction of the exposed skydome
θ_s	angle between the normal to the surface and the sun-target path
θ_{sky}	angle between the normal to the earth and the specularly reflected ray from the sensor to target cast.
θ_b	angle between the normal to the background and the target hit point
θ_{bt}	angle between the normal to the background and the target hit point
θ_v	angle between the normal to the target surface and the sensor-target surface path
θ_E	angle between the normal to the earth at the target and the sensor-earth path

table 1 Definitions of variables in current radiance algorithm

3.6. DIRSIG and Reflectivity

As stated, the current DIRSIG treatment of reflectivity allows for either ideal specular OR ideal diffuse behavior. In reality, most objects' reflectivities exhibit some mixture of specular AND diffuse characteristics. The real reflectivities carry a strong dependence on illumination and view angle that result in phenomenon such as varied specular lobe width, backscatter peaks, and "grazing" angle peaks.

When surfaces are treated as ideal, objects listed as specular exhibit excessive energy reaching the sensor. Objects listed as diffuse often exhibit too little. These effects have been observed in two DIRSIG studies evaluating performance in the thermal infrared (Rankin, 1992) and midwave infrared (Mason, 1993). It is intuitive that these same problems will exist in the visible region.

With the DIRSIG algorithm designed for operation in the thermal region, the reflectivity values are actually derived from a surfaces' angular hemispheric emissivities. The angular hemispheric emissivity values are dependent on view angle only. However, the desired reflectivity is a function of both view angle and illumination angle. Therefore, the conservation of energy law should not apply for BRDF values and angular hemispheric emissivity. A different technique of deriving reflectance values will obviously need to be applied for operation in the visible region. The derivation and application of such a technique will be addressed by this study.

4.0 Approach

The objectives of modifying the DIRSIG radiance algorithm with regards to reflectance *and* evaluating its performance in the visible region, are to be accomplished by the following tasks:

- Practically modify the radiance algorithm
- Obtain ground truth image data
- Generate reflectance data for use by the modified algorithm
- Generate synthetic images using the modified algorithm
- Compare synthetically generated images against ground truth images to evaluate the model's performance

4.1. Modified Radiance Algorithm and Associated Reflectance Values

Practically modifying DIRSIG's treatment of reflectance demands the new technique to be simple to implement. The two areas of interest are the overall radiance algorithm and the characteristic reflectance values used by the algorithm. Easy implementation will be realized if the same *basic* rendering method is retained. Therefore, ray tracing will still be employed to determine the reflected radiance from ideal diffuse and ideal specular surfaces. The major changes will focus on how the radiance algorithm uses the information from the ray tracing and what reflectance values are employed. Minor changes will be recommended on handling solar effects, as well as illumination from a background object.

4.1.1. Radiance Algorithm

As stated, the model assumes each surface is either ideally

specular or ideally diffuse, and uses view angle dependent reflectance values calculated from angular emissivities. However, the modified radiance algorithm will consider each surface as having both specular and diffuse reflectivity characteristics. These characteristics will be represented by two view angle dependent components, R_s and R_d , which are based on actual laboratory reflectance measurements. The support for this treatment is described in section 4.1.4.

The diffuse radiance components will be computed using ray tracing techniques identical to those used currently for diffuse objects. The specular radiance components will also be calculated using similar techniques to those used currently for specular objects. These two radiance components will simply be added to find the total radiance reflected from the target surface. The total energy reaching the sensor for a particular primary ray is found by adding the appropriate atmospheric upwelled radiance to this sum. The modified algorithm is given in equation 4.1. and the new variables are defined in table 2.

An exception for the specular component involves the treatment of incident solar energy. The effects of the sun are considered the same for each surface type, irrespective of what azimuthal plane it's rays follow with respect to the sensor-target plane. This is inappropriate in the visible spectrum due to the bidirectional dependence on reflectivity. Therefore, the modified DIRSIG will treat the solar effects differently for the diffuse and specular components. For the diffuse, the effects will be treated as before,

modified by the diffuse reflectance component. For specular, if the secondary ray actually intersects the sun, within some predefined solid angle, the solar effect is included as modified by the specular reflectance component. If no intersection is made, then the specular component is omitted. An attempt will be made to address the validity of this assumption by analyzing complete BDRF data.

Besides addressing the treatment of the primary object's reflectivity, a change is proposed on how the basic DIRSIG algorithm treats the effects of the illumination from a background object. Currently only the reflection of solar illumination from a background is accounted for. The reflection of the downwelled radiance of the sky as an illumination factor should be included as well. When the sun is no longer illuminating the background, the sky radiance may still be sufficient enough to be a factor. Note that the background object is still always considered diffuse to limit the extent of the calculations. This limitation effects only a small percentage of the overall radiance and thus only adds a small percentage of the error.

Modified Algorithm

L = Specular Component

+ Diffuse Component

+ Upwelled Component

= ((solar + downwelled + background) (specular reflectance)

+ (solar + downwelled + background) (diffuse reflectance)) atm transmission

+ upwelled radiance

= $\left\{ \left[\left(\frac{E_s}{\pi} \right) I'_s \tau_1 \cos \theta_s + L_d(\theta_{sky}) \tau_{bsp} + \left(\left(\frac{E_s}{\pi} \right) I'_b \tau_1 \cos \theta_b + F L_{dsky} \right) R_{db}(\theta_{bl}) (1 - \tau_{bsp}) \right] R_s(\theta_v) \right.$

$\left. + \left[\left(\frac{E_s}{\pi} \right) I'_t \tau_1 \cos \theta_s + F L_{dsky} + (1-F) \left(\left(\frac{E_s}{\pi} \right) I'_b \tau_1 \cos \theta_b + F L_{dsky} \right) R_{db}(\theta_{bl}) \right] R_d(\theta_v) \right\} \tau_2(\theta_E)$

+ $L_u(\theta_v)$

(4 . 1)

$R_s(\theta_v)$	specular component of the angular dependent reflectivity
$R_d(\theta_v)$	diffuse component of the angular dependent reflectivity
$R_{db}(\theta_{bt})$	diffuse component of the angular dependent reflectivity of the background
L	spectral radiance reaching front of the sensor
L_{dsky}	downwelled spectral radiance due to scattering integrated over the skydome
$L_d(\theta_{sky})$	directional downwelled spectral radiance due to scattering
$L_u(\theta_v)$	upwelled spectral radiance due to scattering along the target-sensor path
E_s/π	exoatmospheric solar spectral radiance
τ_1	atmospheric spectral transmission along the source - target path
$\tau_2(\theta_v)$	atmospheric spectral transmission along the target-sensor path
τ_{bsp}	transmission of an object in the target-sky specular bounce direction
I_t	target sun/shadow flag (1 or 0)
I_b	background sun/shadow flag (1 or 0)
I_s	specular incidence/sun intersection flag (1 or 0)
F	shape factor, the fraction of the exposed skydome
θ_s	angle between the normal to the surface and the sun-target path
θ_{sky}	angle between the normal to the earth and the specularly reflected ray from the sensor to target cast.
θ_b	angle between the normal to the background and the target hit point
θ_{bt}	angle between the normal to the background and the target hit point
θ_v	angle between the normal to the target surface and the sensor-target surface path
θ_E	angle between the normal to the earth at the target and the sensor-earth path

Table 2 Definitions of variables in current radiance algorithm

4.1.2. Reflectivity Components

The characteristics of the specular and diffuse reflectance components should exploit how they are employed within the ray tracer and radiance algorithm. The variations of reflectance due to the illumination and viewing angles demand some degree of geometric dependence be represented in the component values. However, the techniques used to interrogate the scene and calculate the radiance put primary dependence on the sensor view angle. In the specular technique, only the energy incident at the ideal specular angle with respect to the view angle is assessed. All other incident energy is assessed by the diffuse technique, which determines the reflected energy incident from the entire hemisphere, for that particular sensor location. For these reasons, the reflectivity components will be view angle dependent.

The radiance algorithm will use the two components to represent the respective percentages of energy reflected to the sensor. In theory, these components are considered complimentary within the total reflected energy, at a view angle. In other words, $R_d(\theta_v) + R_s(\theta_v) = R(\theta_v)$.

4.1.3. Generation of the Reflectivity Components

The true challenge is generating these view angle dependent, reflectivity components for a particular surface. Unfortunately, the literature doesn't contain reflectance models describing reflectivity as it is required by DIRSIG. However, the fundamentals followed by the ERIM hybrid approach will be applied in a general way.

The ERIM method will generate a BRDF value by applying a small subset of polarization dependent BRDF measurements and known surface parameters to a theoretical reflectance model. In contrast, the proposed method will generate view angle dependent, reflectance components (diffuse and specular) by interpolating within a view angle dependent reflectance component database. This component database will be created by applying a series of simple, unpolarized, in-plane BDRF (not BRDF) measurements to a number of assumptions and/or approximations. This highly empirical approximation method is much less stringent than ERIM's. However, ERIM's goal was to determine actual BRDF values and our goals are to create view angle dependent reflectivity components that will incorporate many important reflectivity effects.

The in-plane BDRF measurements will be accomplished using the DIRS Lab's BDRF apparatus and techniques (Feng, 1990). Each scan will accommodate a particular bandpass and illumination angle (75 to 0), while scanning the view angles (-8 to 90 to +8).

Therefore, 20 in-plane scans would be done per material, each scan having 11 measurements.

bandpass (blue,green,red,NIR)	4
illumination angle (8,30,45,60,75)	5
view angles (8,30,45,60,75,90,-75,-60,-45,-30,-8)	11

Each of these in-plane scans will result in a profile as in figure 4.1. The height of the profile at the non-specular lobe

angles will be used to derive the diffuse components. The added height of the profile at the specular angle will be used to calculate the specular component. The size and shape of the lobe represents the directional diffuse characteristics which will be incorporated into the diffuse component.

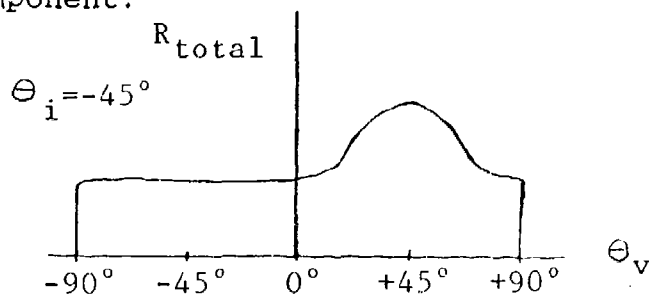


figure 4.1 In-plane reflectance profile (illum angle = -45)

The desired database for a material's reflectivity components will resemble the following table (in structure):

MATERIAL: TRUCK

θ_v	BLUE		GREEN		RED		NearIR	
	Rd	Rs	Rd	Rs	Rd	Rs	Rd	Rs
0.0	.44	.55	.44	.55	.44	.55	.44	.55
1.0	.55	.66	.55	.66	.55	.66	.55	.66
2.0	.58	.68	.58	.68	.58	.68	.58	.68
3.0	.60	.70	.60	.70	.60	.70	.60	.70
4.0	.61	.72	.61	.72	.61	.72	.61	.72
5.0	.63	.73	.63	.73	.63	.73	.63	.73
.
.
90.0	.86	.84	.86	.84	.86	.84	.86	.84

Generating $R_d(\theta_v)$. $R_d(\theta_v)$ is the view angle dependent, diffuse reflectance value component for a particular object. These values will be determined as follows. For each illumination angle, the reflectance value will be measured at each "non specular" view angle. The values from all illumination angles measured for a particular view angle will be averaged to provide an estimate of that view angle's diffuse reflectance. This "weighted" averaging incorporates the lobe width effects into the diffuse reflectance component values.

Incorporating effects of the lobe width better account for the proportion of incident energy actually reflected to the sensor. If energy is incident within the width of the specular lobe (located opposite of the view angle), then more of that energy will be reflected by the surface into that view angle. The surface with a wider, more diffuse lobe, will have a larger amount of incident energy diffusely reflected then the highly specular surface. This is shown by looking at a theoretical "in-plane" reflectivity profile for a particular illumination angle (see figure 4.2).

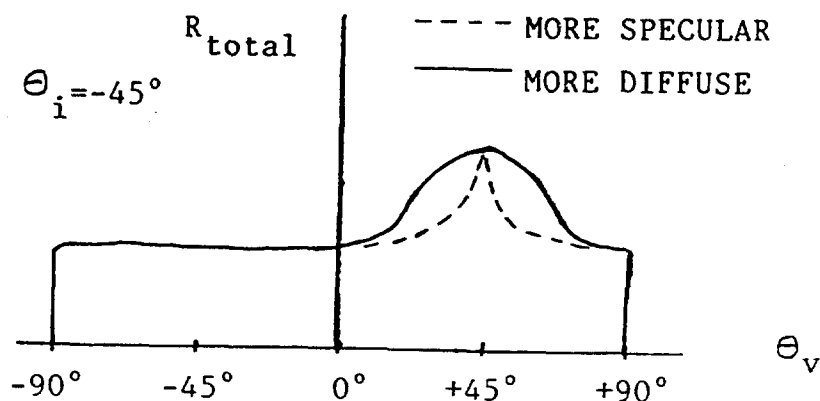


figure 4.2 In-plane reflectance profile (illum angle = -45)

Generating $R_s(\theta_v)$. $R_s(\theta_v)$ is the view angle dependent, specular reflectance value component for a particular object. These values will be determined as follows. For each illumination angle, the reflectance value will be measured at the corresponding "specular" view angle. In other words, for each θ_v , the value where the illumination angle is equal to $-\theta_v$. These 6 values will be determined for 0 to 90 degrees and then symmetry will be assumed to establish the values from 90 to 180 degrees. Finally, the value at each view angle will be subtracted by that view angle's angular diffuse value found previously. The resulting values are the specular components of that view angle's reflectance.

What about materials not easily measured? In many instances, samples of scene objects will not be conducive to laboratory analysis and therefore in-plane BDRF values will not be available. A method must then be established to generate appropriate view angle dependent reflectance components. I propose that an ideal view angle dependent reflectivity component curve be established for each of five categories of reflectivity. These categories can be: highly specular, mostly specular, combination of specular and diffuse, mostly diffuse, and highly diffuse. For a given material, an appropriate curve will be used which is shifted based on a total diffuse reflectance value provided for the object. These curves will be generated somewhat empirically based on the BDRF measurements of the sample materials.

4.1.4. Validity of Reflectance Generation Method

As stated, no established reflectance model exists to provide the type of values required by DIRSIG. The method that will be applied accounts for a majority of the effects described in the Torrence-Sparrow, Cook-Torrence, and He, *et al*, models. These models were theoretical and therefore concerned with "creating" the effects from surface properties. Even ERIM focuses on generating the reflectivity effects theoretically, since their actual reflectance measurements only provide the degree of specularly for a surface. This proposal's method relies directly on the reflectivity effects displayed in actual BRDF measurements. The reflectivity effects are therefore inherent in the data!

Many approximations were applied in describing how the reflectance component database should be generated from the BRDF data. Still, the important physical tendencies that characterize reflectivity will be present. Any errors resulting from these assumptions should fall within the magnitude of errors inherent within practical use of DIRSIG. Under normal use, most of the materials within the scene will not be represented in the database. Therefore, a degree of error will be present from simply using similar material type databases.

Most importantly, it is not a requirement to apply highly accurate reflectance values to a practical SIG model used for remote sensing applications. "The collection of BRDF data is not an end to itself, but rather only one step in the understanding of the radiative transfer of complex objects (targets and backgrounds)....We

must balance our consideration of BRDF (its accuracy, etc.) with respect to the other parameters (sensors, backgrounds, atmosphere, etc.) that also influence the performance of the exploitation technology. BRDF measurements and models are important but represent only one aspect of the exploitation technology that is our central focus" (Arnold and Beard, 1989).

4.2. Obtain Truth Data

The ground truth data for this study will consist of a series of actual images of a scene collected from a fixed view angle over varying solar orientations. The scene will be constructed at ground level just outside the Chester Carlson building and will be imaged from sensors located on the building's roof.

4.2.1. The Scene

The scene will be established to test the capability of DIRSIG in addressing radiance-surface interactions. Figures 4.3 and 4.4 display diagrams of the scene set-up. The primary object groups are the control panels, the shed/specular panel, and the truck/blacktop. The diffuse control panels will provide a standard within the scene and are located at an angle normal to the sensor. The shed front is diffuse and divided into two highly contrasting grey levels. This contrast surface is placed directly behind a flat specular panel to provide a good area to observe background interactions. The truck and blacktop combination will allow for observing shadow interactions as well as background effects. The other objects are in the scene to provide pertinent data to a separate validation study of DIRSIG's thermal infrared capabilities accomplished concurrently. These objects will also be used, where appropriate, to assess DIRSIG's visible region capabilities.

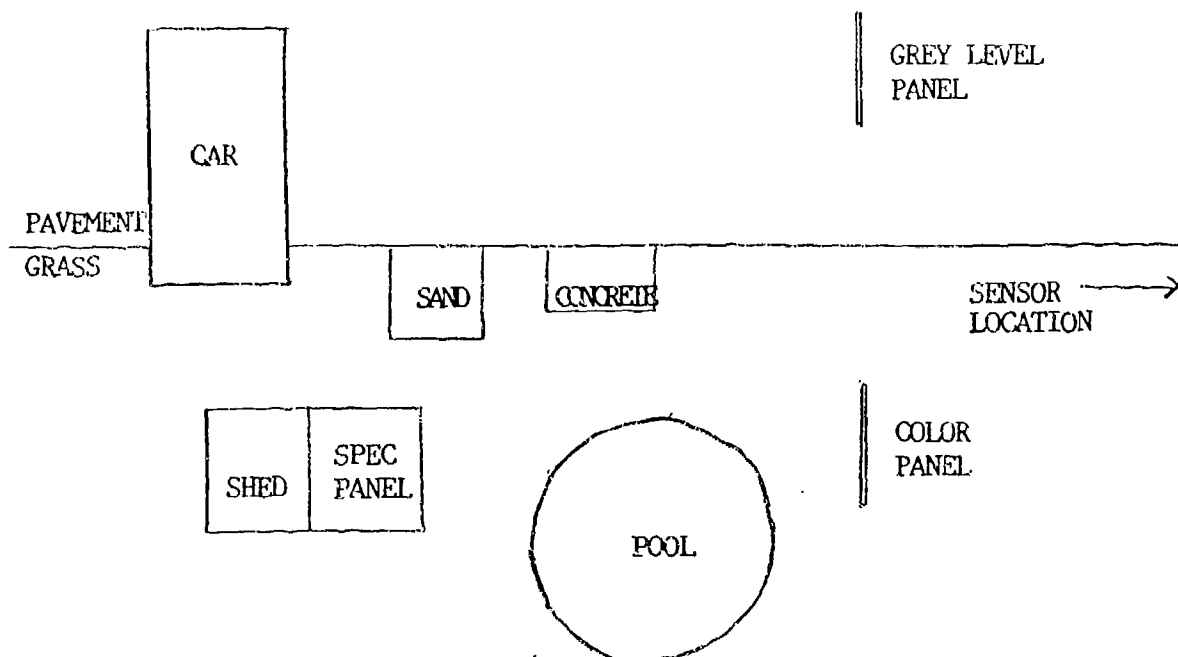


figure 4.3 top view diagram of scene

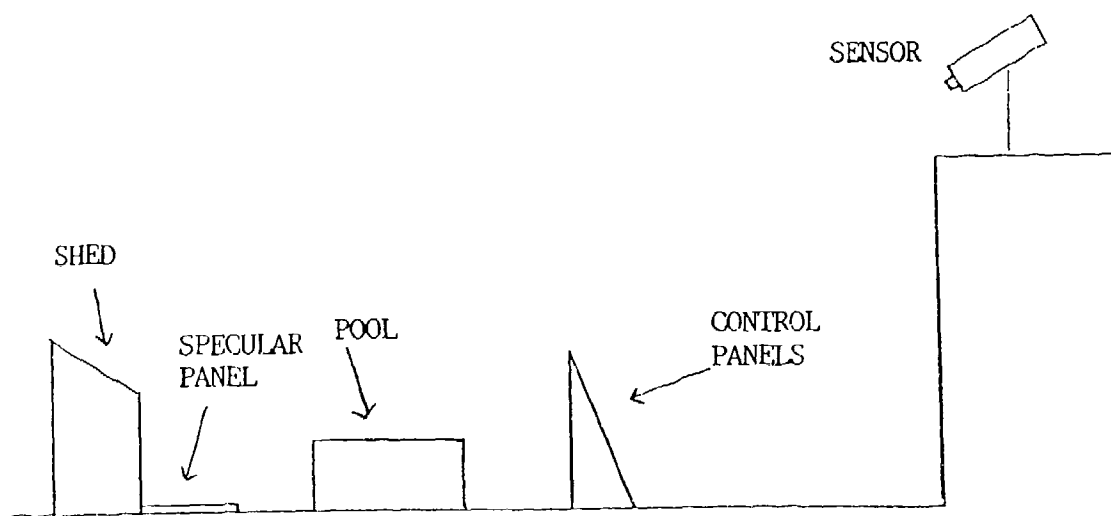


figure 4.4 side view of scene

4.2.2. Image Collection

The images will be detected with a CCD monochrome frame transfer sensor and then digitally stored. A series of four filters will be cycled through to pass only certain bands within the visible spectrum:

blue	420 - 520	nm
green	500 - 580	nm
red	600 - 750	nm
near IR	740 - 1000	nm

Images will be collected in all four bands every 30 minutes from sunrise until sunset to provide a variety of solar illumination angles.

4.2.3. Associated Environmental Data

Besides the actual image data, two atmospheric measurements will be taken concurrently to allow comparisons with derived values by the DIRSIG model. Downwelled radiance measurements will provide both hemispheric and directional downwelled radiance values to compare with DIRSIG. In-scene radiance measurements will provide scene-to-sensor upwelled radiance and atmospheric transmissivity for comparison purposes.

A series of directional downwelled radiance measurements will be made over the sky using a linear array spectrometer located on the roof. Readings will be recorded at nadir plus 6 different elevations each along the north, south, east, and west. These 25 readings will be integrated to provide an estimated value of the hemispheric downwelled radiance during the collection for each of the four

wavelength bands of interest. Estimated values of the directional downwelled radiance within each of the four bands can be obtained by interpolating the 25 readings.

In-scene radiance measurements will be recorded for each of the grey level and RGB panels using a simple radiometric detector. A series of four filters identical to the CCD camera filters will be cycled through for each panel. The intent of this measurement is to collect the radiance as close as possible to the object without blocking a significant amount of illumination. These radiance measurements will be used in conjunction with the concurrent image radiance values for the panels to calculate scene-to-sensor upwelled radiance and atmospheric transmissivity for each of the four wavelength bands. Figure 4.5 shows the relationship between the radiance reaching the sensor, the in-scene object radiance, the upwelled radiance, and the transmissivity.

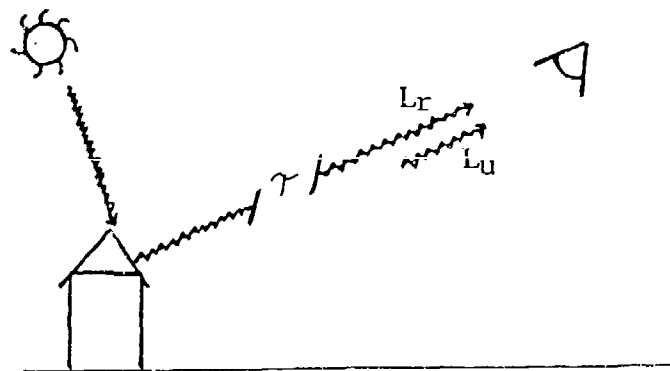


figure 4.5 Radiance reaching the sensor

Two other sources of environmental data will be acquired to provide relevant input to DIRSIG. These are radiosonde data from the Buffalo NWS and weather data from the Rochester NWS. The radiosonde

data provides an atmospheric profile which includes temperature, pressure, and dew point at various elevations. The weather data provides a source of local weather history to relate to any possible anomalies observed in the ground truth images.

4.2.4. Equipment Calibrations

When DIRSIG is run, the output will provide digital counts at each pixel which represent the absolute radiance reaching the front of the sensor. The digital counts stored for the truth data images represent the relative radiance reaching the detector. Therefore, in order to compare the images, the truth data digital counts must be calibrated against a known source to account for the camera and allow transformation to absolute radiance reaching the front of the sensor.

The calibration will be set-up using a known source, a series of neutral density diffuse filters, the appropriate wavelength band filters, and the camera system all aligned on an optical bench. Average pixel digital counts are then recorded for each known radiance level exposed to the front of the camera system. The known radiance levels are produced using the standard source, stepwise attenuated with the neutral density filters. To assess this calibration, it is very important to know exactly what the radiance is reaching the front of the sensor. Thus, the attenuation effect from the filters between the standard source and the sensor must be adequately known.

A relationship between pixel digital count and radiance at the front of the sensor will be established by linear regression.

Considerable attention will be put into manipulating this data correctly to ensure a proper relationship is found. This relationship will be very crucial in making an accurate comparison. If the relationship does not appear adequately linear, then statistical tests will be performed to measure the linear relationships strength.

A similar calibration will be performed on the portable QED radiometer. The radiometer output represents relative radiance reaching the detector. The calibration will allow this data to be transformed into absolute radiance reaching the front of the detector. Therefore, the transformed data can be used to calculate the scene-to-sensor upwelled radiance and transmissivity as described previously.

The photoresearch array spectrometer used in measuring the downwelled radiance, provides accurate absolute radiance values and will be precalibrated.

4.3. Reflectance Measurements

In order to run the DIRSIG software, a database of angular reflectivities are required for each material type of interest within the scene. The main problem with such a data base is that it doesn't exist! For completeness, I'll measure both the diffuse reflectance and the complete hemispheric bidirectional reflectance for appropriate object samples.

The diffuse reflectivity of each sample will be measured using a spectrophotometer and integrating sphere. The spectral output

consists of 5 nm increments from 350 - 900 nm. The output is only available in a graphical form, thus the band pass values will have to be interpreted.

The full bidirectional reflectivity of each sample will be measured using a modified goniospectrometer as described by Feng (1990). This data will be measured for each wavelength channel since the same filters used by the CCD camera will be used for the BDRF detector. In fact, the detector used will be the same QED used to measure the in-scene radiance.

For the sample of the automobile, it will be impractical to bring a portion into the laboratory. Thus, a sample with similar characteristics will be constructed and this sample will be measured as described above for diffuse and bidirectional reflectance. A relation between the sample and the actual truck will hopefully be established by measuring the diffuse reflectivity of the truck with a portable spectrometer and integrating sphere. The spectral output consists of 10 nm increments from 400 - 700 nm. A degree of extrapolation will need to be performed for the 700 - 1000 nm region.

4.4. Generation of Synthetic Images with Modified DIRSIG

Generate synthetic images of the ground truth scene with the modified DIRSIG model. To adequately evaluate the performance of the model, the following will be accomplished:

Match as closely as possible the geometry and dimensionality of the scene model with the actual scene

410
Include the object reflectance values generated as described

Include the appropriate atmospheric data

Generate a series of images from sunrise to sunset to allow evaluation of many different solar illumination effects

4.5. Evaluate Performance

The main objective of this evaluation is to assess the light-surface interactions. Many other parts of the model, such as ray tracing and atmospheric simulation, have already been validated. Most image generator errors are image-wide, object independent anomalies. These types of errors are of interest and will be discussed. However, the object surface reflection errors are of primary interest. These errors may result in severe image degradation such as saturation or contrast reversal.

The assessment will be accomplished by both a qualitative and quantitative evaluation. The qualitative assessment will discuss how well the model handled various physical interactions within the scene. All images generated from sunrise to sunset will be used. The quantitative assessment will focus on the subset of the generated images which have associated high quality ground truth images. The values of per pixel radiance reaching the sensor for a given object will be compared between synthetic and control images.

The quantitative assessment will include an attempt to separate the model errors due to calculated atmospheric data and those due to the treatment of the reflectance. An estimate will be made of the percentage of error in the radiance calculations caused by the model's calculation of the downwelled radiance, upwelled radiance,

and atmospheric transmission. This will be accomplished by comparing the model's L_u , L_d , and T to those measured during the collection. The total error contribution of non reflectance effects can be determined via Beer's Law analysis (Beer, 1957). Removal of these sources of error will allow the reflectance error to be better evaluated.

The relative surface reflectance errors will then be assessed by plotting the synthetically generated pixel digital counts verses the calibrated ground truth pixel digital counts. A linear regression will be performed on the relation and plotted along with a "unity" line. If the data falls randomly about unity as in figure 4.6, these variations will be due to the errors in the treatment of surface reflectance. If the data points deviate from unity, as in figure 4.7, then there is some type of linear error. Such error will most likely be from calibration, since the effects of atmospheric transmission and upwelled radiance should be relatively small. To compensate for this error, the original synthetic pixel digital counts will be transformed through the regression line and then replotted against the truth data. This will remap the variations about unity as previously described, without inclusion of calibration error effects.

Another possible assessment for the degree of reflectance error can be made by looking at the validity of certain assumptions used in generating the reflectance components. For this, the full-BRDF data of various sample objects can serve as the ground truth for. Note, the generated reflectance component values do not represent the same

combination of effects as the measured full-BRDF values and therefore shouldn't be directly compared to each other.

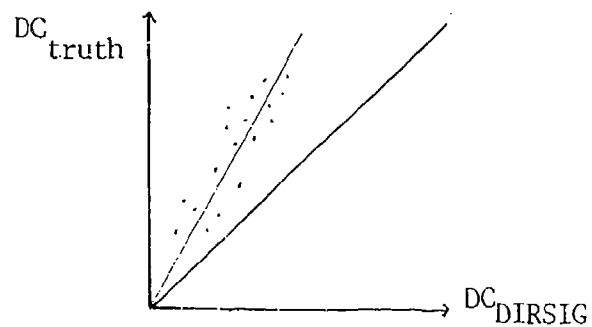


figure 4.6 Synthetic DC verses Truth DC with linear error

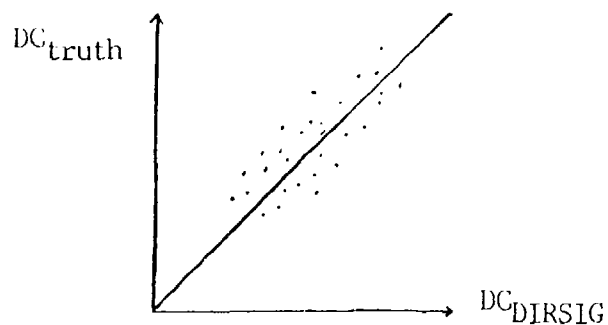


figure 4.7 Synthetic DC verses Truth DC with no linear error

Qualitatively, the most important feature will be how well the relative contrast effects within the scene were handled by the model. For instance, the light and dark panels of the shed should be correct when viewed directly, or when viewed within the specular reflection. Other qualitative effects, like specular glint, can be described when viewing the images side-by-side. The assessment of these effects will be made at each of the particular spectral bands to determine relative capabilities. However, the overall realism for the visible image can further be determined by comparing combination images created by adding together the red, green, and blue images.

5. SUMMARY

This study focuses on operation of the RIT DIRSIG model within the 0.4 to 1.0 μm wavelength region. Modifications will be made to DIRSIG's treatment of radiance-surface interactions and then the model output will be assessed. The modifications will involve altering the radiance algorithm as well as identifying more realistic material reflectance values. The performance evaluation will be accomplished by collecting truth data from an actual scene and comparing it to data from a synthetically generated image of the same scene. This evaluation will serve as a first overall assessment of the model's performance in this wavelength region and is intended to set the groundwork for future enhancements.

6. TIMETABLE

	92								93							
	May	Jun	Jul	Aug	Sep	Oct	Nov	Dec	Jan	Feb	Mar	Apr	May	Jun		
Dev New Method	x	x	x	x	x	x	x	x								
Obtain Truth	x	x	x						x	x	x					
Obtain Reflec		x	x	x	x	x										
Apply New Method										x	x	x				
Findings											x	x	x			
Write Thesis												x	x	x		

7. References

Arnold, C.B. and J.L. Beard, "An ERIM perspective on BRDF measurement technology," *Scatter from Optical Components*, J.C. Stover, Editor, Proc. SPIE 1165, pp 112-135 (1989)

Beers, Y., Introduction to the Theory of Error, Addison-Wesley Publishing Company, Inc., Reading Mass., 1957

Blinn, J.F., "Models of Light Reflection for Computer Synthesized Pictures," *Computer Graphics*, Vol 11, No 2, pp 192-198, July 1977

Bouville, C. and K. Bouatouch, "Developments in Ray Tracing," Advances in Computer Graphics IV, Eurographic Seminars, W.T. Hewitt, M. Grave, and M. Roch (editors), Springer-Verlag, New York, 1991

Cathcart, J.M., A.D. Sheffer, and W.L. Wooten, "Synthetic Visible Imagery for Multi-Attribute Target Identification," *Signal and Image Processing Systems Performance Evaluation*, SPIE 1310, pp 150-160 (1990)

Cook, R.L. and K.E. Torrence, "A Reflectance Model for Computer Graphics," *ACM Transactions on Graphics*, Vol 1, No 1, pp 7-24, January 1982

Environmental Institute of Michigan, "Polarized Emittance Vol 1: Polarized Bidirectional Reflectance with Lambertian or Non-Lambertian Diffuse Components," prepared for the USA Ballistic Research Laboratories (BRL), BRL Contract Report No 154, May 1974

Feng, X., J.R. Schott, and T. Galligher, "Comparison of Methods for Generation of Absolute Reflectance Factor Values for BRDF Studies," submitted for journal publication by Rochester Institute of Technology, Center for Imaging Science, November 1992

Feng, X., "Comparison of methods for generation of absolute reflectance factor measurements for BRDF studies," M.S. Thesis, Rochester Institute of Technology, Center for Imaging Science, December 1990

Goral, C.M., K.E. Torrence, D.P. Greenberg, and B. Battaile, "Modeling the Interaction of Light Between Diffuse Surfaces," *Computer Graphics*, Vol 18, No 3, pp 213-222, July 1984

Greenberg, D.P., "Light Reflection Models for Computer Graphics," *Science*, Vol 244, pp 166-173, April 1989

He, X.D., K.E. Torrence, F.X. Sillion, and D.P. Greenberg, "A Comprehensive Physical Model for Light Reflection," *Computer Graphics*, Vol 25, No 4, pp 175-186, July 1991

Lillesand, T.M. and R.W. Kiefer, Remote Sensing and Image Interpretation, 2nd ed., John Wiley and Sons, Inc., New York, 1987

-46-

Lindahl, C., A. Cockcroft, T. Derryberry, J. Sigler, and M. Yablonski, "Synthetic, multisensor, database generation and validation," *Signal and Image Processing Systems Performance Evaluation*, SPIE 1310, pp 88-94 (1990)

Magnenat-Thalmann, N. and D. Thalmann, Image Synthesis: Theory and Practice, Springer-Verlag, New York, 1987

Mason, J., "DIRSIG Validation in the Mid-Wave Infrared Region," Presentation at DIRS Lab Meeting, Rochester Institute of Technology, Center for Imaging Science, December 1992

Nicodemus, F.E., "Directional Reflectance and Emissivity of an Opaque Surface," *Applied Optics*, Vol 4, No 7, pp 767- 772, July 1965

Rankin, D., "DIRSIG Validation in the Long Wave Infrared Region," Presentation at DIRS Lab Meeting, Rochester Institute of Technology, Center for Imaging Science, November 1992

Raqueno, R., C. Salvaggio, J.S. Warnick, E. Kraus, and J.R. Schott, "A thermal infrared synthetic image generation model," Final Report RIT/DIRS 90/91-63-142, prepared for the Central Intelligence Agency, Office of Development and Engineering, April 1991

Reeves, R., D. Anding, and F. Mertz, "First-Principles Deterministic Simulation of IR and Visible Imagery," *Multispectral Image Processing and Enhancement*, SPIE 933, pp 207-230 (1988)

Salvaggio, C., G. Braun, and J.R. Schott, "SVGM: a spectral vector generating model using the LOWTRAN 7 and SCATRAM atmospheric propagation codes," RIT/DIRS 90/91-63-141, prepared for Eastman Kodak Company, Federal Systems Division, January 1991

Schott, J.R., M. Fairchild, X. Feng, R. Raqueno, B. Brower, and T. Galligher, "Techniques for measurement of the optical properties of materials," Final Report RIT/DIRS 89/90-51-134, prepared for United States Department of Energy, January 1990

Sillion, F.X., J.R. Arvo, S.H. Westin, and D.P. Greenberg, "A Global Illumination Solution for General Reflectance Distributions," *Computer Graphics*, Vol 25, No 4, pp 187-195, July 1991

Torrence, K.E. and E.M. Sparrow, "Theory of Off-Specular Reflection From Roughened Surfaces," *Journal of the Optical Society of America*, Vol 57, No 9, pp 1105-1112, September 1967

Wallace, J.R., M.F. Cohen, and D.P. Greenberg, "A Two-Pass Solution to the Rendering Equation: A Synthesis of Ray Tracing and Radiosity Methods," *Computer Graphics*, Vol 21, No 4, pp 311-320, July 1987